

Prospects for Silicon Mid-IR Raman Lasers

Bahram Jalali, *Fellow, IEEE*, Varun Raghunathan, *Student Member, IEEE*, Ramesh Shori, Sasan Fathpour, *Member, IEEE*, Dimitrios Dimitropoulos, and Oscar Stafsudd, *Senior Member, IEEE*

(Invited Paper)

Abstract—This paper presents the case for the silicon Raman laser as a potential source for the technologically important mid-wave infrared (MWIR) region of the optical spectrum. The mid-IR application space is summarized, and the current practice based on the optical parametric oscillators and solid state Raman lasers is discussed. Relevant properties of silicon are compared with popular Raman crystals, and linear and nonlinear transmission measurements of silicon in the mid-IR are presented. It is shown that the absence of the nonlinear losses, which severely limit the performance of the recently demonstrated silicon lasers in the near IR, combined with unsurpassed crystal quality, high thermal conductivity and excellent optical damage threshold render silicon a very attractive Raman medium, even when compared to the very best Raman crystals. In addition, silicon photonic technology, offering integrated low-loss waveguides and microcavities, offers additional advantages over today's bulk crystal Raman laser technology. Using photonic crystal structures or microring resonators, the integrated cascaded microcavities can be employed to realize higher order Stokes emission, and hence to extend the wavelength coverage of the existing pump lasers. Exploiting these facts, the proposed technology can extend the utility of silicon photonics beyond data communication and into equally important applications in biochemical sensing and laser medicine.

Index Terms—Er:YAG and erbium-based solid-state lasers, mid-IR silicon lasers, midwave infrared (MWIR) silicon laser, silicon Raman lasers, two-photon absorption (TPA).

I. INTRODUCTION

COMPACT, broadly tunable, energy efficient midwave infrared (MWIR)/ longwave infrared (LWIR) sources have been the topic of active research for over two decades. Historically, the need for sources operating in the 3–5- and 8–12- μm atmospheric transmission windows has been primarily driven by military applications such as wind light detection and ranging (LIDAR), remote chemical and biological sensing, and IR countermeasures (IRCM). However, over the past decade, such sources have also found use in a wide array of applications ranging from purely scientific uses, such as ring down and Fourier transform infrared (FTIR) spectroscopy, to clinical uses where tissue ablation is achieved by targeting the resonant absorption peaks in water, the amide bonds in collagen, and other tissue chromophors in the MWIR region. Additionally, industrial uses such as hydrocarbon detection from vehicles, oil fields, and industrial smoke stacks are of interest.

Manuscript received November 17, 2006. This work was supported in part by the Defense Advanced Research Projects Agency and in part by Northrop Grumman Corporation.

The authors are with the Department of Electrical Engineering, University of California, Los Angeles, CA 90095-1594 USA (e-mail: jalali@ucla.edu; varun@ee.ucla.edu; rshori@ee.ucla.edu; sasan@ee.ucla.edu; ddmitr@ee.ucla.edu; stafsuidd@ucla.edu).

Digital Object Identifier 10.1109/JSTQE.2006.885340

The maturing diode pumped solid state lasers technology combined with continued improvements of IR transmitting nonlinear crystals, especially with respect to the reduced bulk absorption at the pump wavelength (typically between 1–3 μm) and the higher damage threshold, optical parametric oscillators (OPOs) have become popular for generating tunable MWIR radiation for many of the above-mentioned applications [1]–[3]. Much effort has been taken on designing the tandem OPO-based system using 1064-nm laser as the pump source [4]–[6]. While these systems use the most mature laser as a pump source (i.e., Nd:YAG laser), the tandem OPO configuration adds considerable complexity to the design and operation of the overall system and often results in significant penalty in terms of the effective electrical-to-optical conversion efficiency, when compared to single-stage OPO systems with the pump laser emitting between 2.1 to 3 μm [7]–[10]. While the advances in nonlinear material, IR coating, and OPO systems level design have resulted in the operation over a broad range of pulse durations [femtosecond pulses–continuous wave (CW)], spectral region coverage, power scaling, and more importantly overall system robustness, such lasers are still a specialty item. OPOs are far from widespread use, primarily due to the high cost and limited commercial availability of high quality MWIR nonlinear crystals. An alternative means to generate MWIR radiation, and one that mitigates some of these limitations, is the solid-state Raman laser (SSRL).

SSRLs have also made remarkable advances in recent years. The development of SSRLs based on crystalline Raman materials pumped at the fundamental and frequency-doubled Nd-based and Ti:Sapphire lasers has resulted in the generation of a broad range of wavelengths ranging from visible up to 1.6 μm , and more impressively, the demonstration of CW Raman laser action at ~ 589 nm with power levels approaching a few watts. Compared to the OPO, the SSRL utilizes a much simpler architecture for IR frequency shifting of the pump [11]. The SSRLs, although not as broadly tunable as OPOs, can be tuned via the pump wavelength. The recent demonstration of the first silicon Raman laser [12] combined with an excellent transmission of silicon in the mid-IR suggests that silicon should be considered as a MWIR Raman crystal. Operating in the 1550-nm near-IR band, the main limitation of silicon Raman lasers at the present is the loss due to free carriers that are generated by two photon absorption (TPA) [13], [14]. Active carrier sweep out using a p-n junction has been proposed as a mean to mitigate this problem [13], [14] and CW operation has been demonstrated using this technique [15]. However, the p-n junction is only partially effective and the remaining free carriers limit the output power to only a few megawatt levels. In addition, this approach causes

the electrical power to dissipate on the Raman crystal, a problem that does not exist in the conventional Raman lasers. However, as will be experimentally shown in this paper, the TPA vanishes in the MWIR regime, hence eliminating the main problem with silicon Raman lasers [16]. This combined with: 1) the unsurpassed quality of commercial silicon crystals; 2) the low cost and wide availability of the material; 3) extremely high optical damage threshold of 1–4 GW/cm² (depending on the crystal resistivity); and 4) excellent thermal conductivity, renders silicon a very attractive Raman crystal.

This paper presents the case for silicon Raman lasers operating in the MWIR. Section II starts with the physics of Raman scattering in silicon followed by a discussion on other nonlinear optical effects that may compete or undermine the stimulated Raman amplification, a prerequisite for lasing. It then provides a comprehensive table that summarizes the key parameters of silicon compared to the currently-used Raman crystals. It is shown that the combination of a high Raman gain coefficient, a large thermal conductivity, and high damage threshold render silicon a superior Raman medium, even when compared to the very best Raman crystals. Section III presents the severe challenges faced by silicon Raman laser, when operated in the near IR. It discusses the popular use of a reverse-biased p-n junction as a means to eliminate the free carrier loss, and shows that electric field screening renders this approach ineffective at moderate and high pump intensities, hence severely limiting the laser output power. It builds the case for pumping at wavelengths longer than that of the two-photon bandedge ($\sim 2.2 \mu\text{m}$) as the most promising approach to exploit the favorable Raman properties of silicon. Section IV validates this concept by presenting new results on the measurements of linear and nonlinear transmission characteristics of silicon in MWIR. Of particular significance, as it relates the prospects for MWIR lasers, is the observed absence of nonlinear losses (two photon and three photon) at intensities of up to $>100 \text{ MW/cm}^2$. Section V discusses self-focusing and thermal-lensing effects, followed by waveguide-design considerations. The possibility of extending the addressable wavelength range of silicon Raman lasers using higher order Stokes emission is presented. It concludes by discussing two candidates for cascaded cavity designs that can enable this capability. Finally, Section VI summarizes the paper.

II. NONLINEAR OPTICS IN SILICON

This section describes the various nonlinear optical processes in silicon. The discussion encompasses Raman, Brillouin, and nonlinear absorption processes including the TPA, three-photon absorption (three-PA), and free-carrier absorption (FCA). Silicon is compared with other popular solid-state Raman crystals to ascertain its place as a MWIR Raman medium.

A. Raman Scattering

A simple and intuitive macroscopic description of the Raman scattering process is as follows. In spontaneous scattering, the thermal vibrations of the lattice at frequency ω_v (15.6 THz in silicon) produce a sinusoidal modulation of the susceptibility. The incident pump field induces an electric polarization that

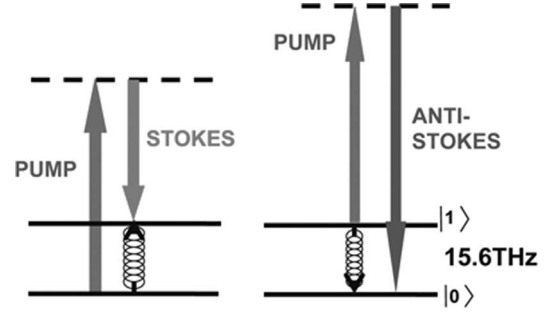


Fig. 1. Stokes and anti-Stokes generation processes in Raman scattering.

is given by the product of the susceptibility and the incident field. The beating of the incident field oscillation (ω_p) with the oscillation of the susceptibility (ω_v) produces induced polarizations at the sum frequency, $\omega_p + \omega_v$, and at the difference frequency $\omega_p - \omega_v$. The radiation produced by these two polarization components is referred to as anti-Stokes and Stokes waves, respectively. Fig. 1 depicts the vibrational energy levels of silicon and the Stokes/anti-Stokes generation processes. Quantum statistics dictates that the ratio of Stokes power to anti-Stokes power is given by $(1 + N)/N$ where

$$N = \left[\exp\left(\frac{\hbar\omega_v}{kT}\right) - 1 \right]^{-1}.$$

N is the Bose occupancy factor and has a value of ~ 0.1 for silicon at room temperature. This model can be extended to describe the stimulated Raman scattering [17]. Here, it is assumed that the pump field and the Stokes field are already present, with a frequency difference equal to the atomic vibrational frequency. The latter is due to the spontaneous emission. The key point is that the two fields (pump and Stokes) create a force that stimulates atomic vibrations, even in the absence of a static dipole moment (such is the case for centrosymmetric silicon crystal). The driving force can be understood as follows. If E is the total field comprising the pump and Stokes field, and χ is the susceptibility, the energy stored in the field $V = (1 + \chi/2)EE^*$ will have a component oscillating at $\omega_p - \omega_s = \omega_v$. Through the modulation of the susceptibility with displacement Q , this will produce a force

$$F \propto \frac{\partial V}{\partial Q} \approx \frac{\partial \chi}{\partial Q} E_p E_s \exp(-\omega_v t).$$

This driving force will enhance the atomic oscillations, which in turn will increase the amplitude of the Stokes field E_s . This positive feedback phenomenon is called stimulated Raman scattering and results in the amplification of the Stokes field.

While the above macroscopic model is intuitively simple to understand, it does not account for the detailed processes responsible for Raman scattering in silicon. The microscopic picture reveals that the direct coupling of light with atomic vibrations is very weak in the near-IR and MWIR wavelengths. This is generally true in semiconductors owing to the large atomic mass. In silicon, the lack of dipole moment further underscores this fact. The electrons mediate the Raman scattering process in silicon. Microscopically, the scattering proceeds in three steps [18]. In

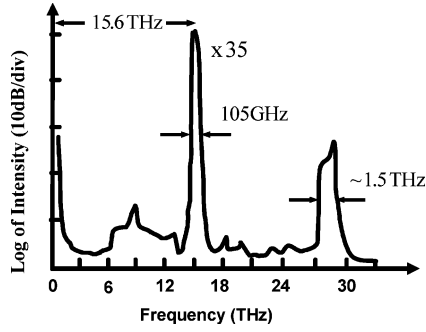


Fig. 2. Spontaneous Raman spectra of silicon showing the first- and second-order Stokes emission (from [19]). Frequency is plotted relative to pump frequency. Anti-Stokes spectrum is not shown.

step 1, the incident photon excites the semiconductor into an intermediate step by creating an electron-hole pair. In step 2, the pair is scattered into another state by emitting a phonon via the electron-phonon interaction Hamiltonian. In step 3, the electron-hole pair in the intermediate step recombines radiatively with the emission of a scattered photon. While electrons mediate the process, they remain unchanged after the process. Furthermore, the transitions involving electrons are virtual, and hence do not have to conserve the momentum, although the energy must be conserved.

Fig. 2 shows the Raman spectrum of silicon [19]. The vibrational modes involved in the first-order Raman scattering process in silicon are the triply degenerated zone-center optical phonons. The pump to Stokes separation is ~ 15.6 THz or 520 cm^{-1} and the bandwidth of the first-order Raman scattering peak is ~ 105 GHz as determined by the optical phonon response time in silicon. The higher order Raman scattering features are much broader, nonetheless weaker than the first-order scattering peak.

Crystal symmetry imposes a selection rule that dictates which scattering geometries are allowed. The spontaneous scattering efficiency S is given by

$$S = S_0 \sum_{k=1,2,3} |\hat{e}_s R_k \hat{e}_p|^2. \quad (1)$$

Unit vectors \hat{e}_p and \hat{e}_s denote the polarization of the pump and Stokes electromagnetic fields. S_0 contains the intrinsic microscopic property of silicon and can be written as

$$S_0 = \frac{k_S^4}{32\pi^2 n} V \left(\frac{da}{dQ} \right)^2. \quad (2)$$

Here, k_S is the Stokes wavevector, n is the refractive index, V is the scattering volume and da/dQ is the derivative of the polarizability with respect to the atomic displacement. Thus, the spontaneous scattering efficiency in free space scales as $1/\lambda_S^4$, similar to the Rayleigh scattering process. In silicon, S_0 has a value of $8.4 \times 10^{-7}/\text{cm}\cdot\text{sr}$ at 1550-nm pump wavelength [20].

The stimulated scattering process is described in terms of the polarization and a macroscopic third-order Raman susceptibility [21]

$$P_i^{(3)}(\omega_S) = \varepsilon_o \chi_{ijkl}^{(3)} E_j(\omega_S) E_k(\omega_p) E_l(-\omega_p). \quad (3)$$

TABLE I
COMPARISON OF VARIOUS RAMAN SOLID-STATE LASER MATERIALS
(FROM [11]) WITH SILICON

Properties of Raman media	Silicon	Ba(NO ₃) ₂	LiIO ₃	KGd(WO ₄) ₂	CaWO ₄
Transmission Range (μm)	1.1-6.5	0.38-1.8	0.38-5.5	0.35-5.5	0.2-5.3
Refractive index	3.42	1.556	1.84 (o) 1.711 (e)	1.986 p[mm]p 2.033 p[gg]p	1.884 (o) 1.898 (e)
Raman shift at 300K (cm^{-1})	521	1047.3	770 822	901 768	910.7
Spontaneous Raman linewidth (cm^{-1})	3.5	0.4	5.0	5.9	4.8
Raman gain (cm/GW)	20 (1550nm)	11 (1064nm)	4.8 (1064nm)	3.3 (1064)	-
Optical damage threshold (MW/cm^2)	~ 1000 -4000	~ 400	~ 100	-	-
Thermal conductivity ($\text{W}/\text{m}\cdot\text{K}$)	148	1.17	-	2.6 [1 0 0] 3.8 [0 1 0] 3.4 [0 0 1]	16

The Raman susceptibility has a typical resonant Lorentzian profile, which peaks at the Stokes/anti-Stokes frequencies.

The evolution of the Stokes intensity along the propagation direction is given by

$$\frac{dI_S}{dz} = g_R I_P I_S$$

where the gain coefficient is determined by the value of the Raman susceptibility

$$g_R = \frac{3\omega_S \mu_o}{n_S n_P} \chi_{ijkl}^{(3)} = \frac{6\pi \mu_o}{\lambda_S n_S n_P} \chi_{ijkl}^{(3)}. \quad (4)$$

The gain coefficient extracted from measurements performed near 1550 nm is $20 \text{ cm}/\text{GW}$ [21]. For application to MWIR, the gain-coefficient scales with wavelength of $1/\lambda_S$ is evident in the above expression.

Table I compares silicon with popular Raman crystals that are presently being used. The latter category includes Ba(NO₃)₂, LiIO₃, KGd(WO₄)₂ and CaWO₄ [11]. It is seen that silicon is quite competitive with these crystals in terms of MWIR transmission range and Raman gain. Thermal conductivity of the crystals is an important parameter in the design of high-power Raman lasers. When this is considered, silicon has superior performance as compared to other crystals.

B. Brillouin Scattering

Stimulated Brillouin scattering occurs at high enough pump intensities at which the acoustic waves are driven by the coherent interaction of the pump and the Stokes waves. The detailed analysis of the Brillouin scattering can be found in [17] and [22]. Brillouin scattering has been observed in fibers and has been used to build ultranarrow-linewidth fiber lasers [23].

In the first measurement of the Brillouin spectrum of silicon, the incident wavelengths used were 488 nm and 632.8 nm [24]. The spectrum of silicon in the backscattering direction with 488-nm wavelength is shown in Fig. 3 (from [24]). The shift has been calculated at telecom wavelengths to be ~ 40 GHz [24], [25], and the spontaneous scattering efficiency has been obtained as $1.2 \times 10^{-8}/\text{cm}\cdot\text{sr}$ [25]. Thus, the spontaneous scattering efficiency for Brillouin is lower than that of the Raman process. The Brillouin scattering linewidth is expected to be of the order

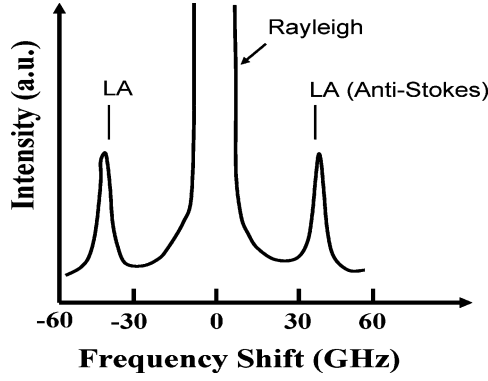


Fig. 3. Spontaneous Brillouin spectrum of silicon as obtained by Sandercock [24] in a backscattering configuration from a (100) surface (normal incidence). The incident wavelength was 488 nm.

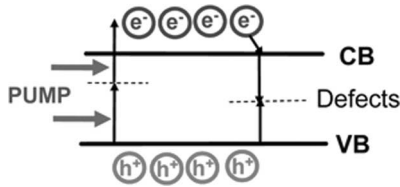


Fig. 4. Two-photon absorption process and the generation of free carriers. If allowed to accumulate, these carriers result in substantial increase in optical loss. The so-called nonlinear loss competes with Raman gain.

of tens of megahertz, thus reducing the Brillouin gain significantly when pumped with the laser sources of bandwidth 100 MHz or higher [23]. Hence, the Brillouin scattering process is not expected to deplete the pump, when trying to observe Raman scattering with sufficiently large pump bandwidth.

C. Nonlinear Absorption Processes

In the presence of high pump intensities required to observe Raman scattering, there are competing nonlinear absorption processes, which could become significant enough to reduce the Raman gain substantially. These are TPA, FCA, and possibly three-PA processes. A schematic of the TPA process and the generation of free carriers are shown in Fig. 4. The TPA has been shown to be negligible from the point of view of pump depletion [21]. This is plausible since the TPA coefficient in silicon β is relatively small ~ 0.5 cm/GW, when compared to the Raman gain coefficient of $g_R = 20$ cm/GW at 1550-nm wavelength. On the other hand, absorption by TPA-generated free carriers is a broadband process that competes with the Raman gain. The magnitude of TPA-induced FCA depends on free-carrier concentration through the relation

$$\alpha^{\text{FCA}} = 1.45 \times 10^{-17} \left(\frac{\lambda}{1.55} \right)^2 \Delta N = \sigma \Delta N \quad (5)$$

where λ is the wavelength of interest (in micrometers), and ΔN is the density of electron-hole pairs [13], [14]. The latter is related to the pump intensity I_p by

$$\Delta N = \frac{(\beta_2 I_p^2 + 2\beta_2 I_p I_S) \tau_{\text{eff}}}{2h\nu} \quad (6)$$

where $h\nu$ is the pump photon energy, and τ_{eff} is the effective recombination lifetime for free carriers. The deleterious impact of free-carrier losses when measuring Raman scattering effects, is discussed experimentally at near-IR wavelengths in Section III, along with the possible solutions to overcome these effects to fully utilize the Raman nonlinear effects.

Another nonlinear absorption process that occurs at high pump intensities and wavelengths less than half the bandgap of silicon is three-PA. The experimental results of nonlinear absorption presented in Section IV clearly indicate that at typical mid-IR wavelengths in the 2.1–2.9- μm range, the three-PA process is insignificant, even at the highest pump intensity of 200 MW/cm² used in our measurements.

The competition of these deleterious effects with Raman gain can be described in the following equations describing the propagation of pump and Stokes intensities:

$$\begin{aligned} \frac{dI_P}{dz} &= -\alpha I_P - g_R I_P I_S - (\beta_2 I_P + 2\beta_2 I_S) I_P \\ &\quad - \alpha_P^{\text{FCA}} I_P - \gamma_3 I_P^3 \\ \frac{dI_S}{dz} &= -\alpha I_S - g_R I_P I_S - 2\beta_2 I_S I_P - \alpha_S^{\text{FCA}} I_S. \end{aligned} \quad (7)$$

In the order of appearance, the equation describing pump propagation includes linear losses, Raman pump depletion, Stokes gain, TPA, TPA-induced FCA, and three-PA. The FCA cross section for TPA process is defined in (5). In the range of intensities considered here, the three-PA effect is negligible as supported by the experimental data of Section IV, and hence $\gamma_3 \approx 0$. FCA losses due to three-PA are also neglected.

A summary of the relevant nonlinear optical effects along with their strength and bandwidth is presented in Table II. It is interesting to note that serendipitously, Raman scattering process is the strongest among these effects.

III. RAMAN SCATTERING IN SILICON AT NEAR-IR WAVELENGTHS

In this section, some of the recent results in the demonstration of amplification and lasing at near-IR wavelengths are described. The deleterious effect of nonlinear loss due to FCA and the various schemes used to mitigate this effect are also elucidated.

A. Raman Gain and Nonlinear Losses

Raman gain and the nonlinear loss mechanisms were discussed in Section II. The evolution of Raman gain and nonlinear losses along the length of the waveguide was solved numerically in (7). The net achievable gain is plotted in Fig. 5 as a function of pump intensity. Calculations are performed for pumping at 1550 nm, where TPA is prominent. The TPA-induced FCA depends on the steady-state free-carrier density, a quantity that is proportional to carrier lifetime τ_{eff} . The results suggest that the carrier lifetime is a central parameter, and lifetimes of a nanosecond or larger severely limit the gain and result in a net loss.

Experimental observation of the behavior predicted by the model is shown in Fig. 6. The figure shows the measured Raman gain under CW pump illumination. A 1.5- μm -wide 2- μm -high

TABLE II
SUMMARY OF PERTINENT NONLINEAR OPTICAL EFFECTS IN SILICON AND COMPARISON OF THEIR RELATIVE STRENGTHS

Nonlinear effect	Description	Strength of nonlinearity	Spectral Properties
Stimulated Raman scattering	Stimulated interaction of optical phonons with the Stokes and a strong pump field	$g_R = 20\text{cm/GW}$ (at 1550nm)	Shift =15.6THz (fixed) Bandwidth = 105GHz (Fixed) Gain scales as $1/\lambda$
Stimulated Brillouin scattering	Stimulated interaction of acoustic phonons with the Stokes field and a strong pump field	$g_B = \frac{2.3}{\Delta f} \text{cm/MW}$ (at 1550nm)	Shift ~40GHz (at 1550nm), scales as $1/\lambda$ Bandwidth = Δf (MHz) – not measured
<u>Nonlinear Absorption</u>			
Two-Photon Absorption	Absorption of 2 photons in succession	$\beta_2 = 0.5\text{cm/GW}$ (at 1550nm)	Similar profile as linear absorption. Cutoff at $2.2\mu\text{m}$ (half band gap)
Three-Photon Absorption	Absorption of 3 photons in succession	$\gamma_3 = \text{much weaker than } \beta_2$	Similar profile as linear absorption. Cutoff at $3.3\mu\text{m}$ (1/3rd band gap)
Free-carrier Absorption	Absorption due to free carriers present/ created in the semiconductor	$\alpha_{FCA} = \sigma\Delta N \sim 1\text{cm}^{-1}$ (at ΔN of $\sim 10^{17}/\text{cm}^3$)	Broadband absorption process. Scales as λ^2 .

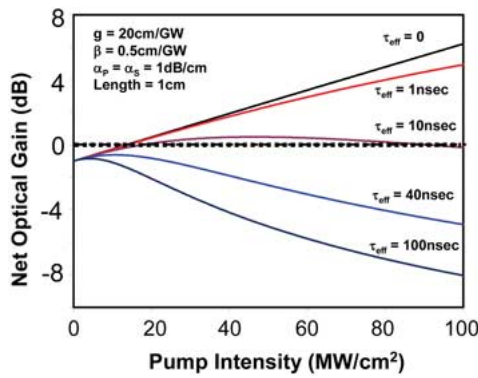


Fig. 5. Evolution of net gain (i.e., Raman gain – nonlinear losses) as a function of input pump intensity. This clearly illustrates the importance of carrier lifetime reduction.

rib waveguide with a length of 2 cm was used in these measurements. A lateral p-n junction straddles the rib with $1.9\text{-}\mu\text{m}$ spacing between the p+/n+ doped region and the rib edge. The waveguide was pumped by CW power at 1427-nm wavelength, and the gain was measured using a second laser beam tuned to the Stokes wavelength of 1542 nm. With the diode open circuited, the accumulation of free carrier results in a net optical loss at the Stokes wavelength. When a reverse bias is applied, the field removes the free carriers reducing their effective lifetime. The maximum gain is obtained at a reverse bias of 10 V. Higher voltages do not increase the gain, a phenomenon that is most likely due to the saturation of drift velocity, a well-known feature of the carrier transport in semiconductor that occurs at a peak electric field of approximately $2 \times 10^4 \text{ V/cm}$. This hypothesis is supported by the fact that for a p-n separation of $5.3 \mu\text{m}$ in our device, the average electric field at 10-V bias is $2.02 \times 10^4 \text{ V/cm}$.

The decrease of gain at higher pump intensities under reverse bias can be attributed to the increase in free-carrier losses due

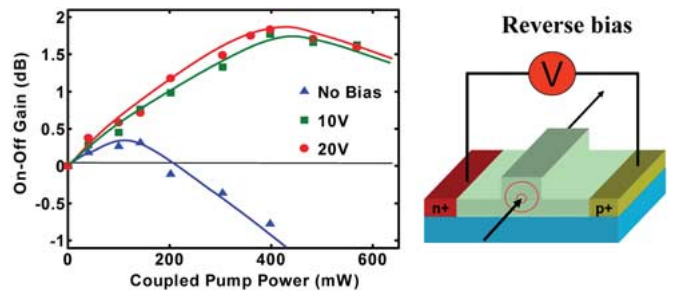


Fig. 6. Measured CW Raman gain for a 2-cm-long waveguide. A lateral reversed-bias p-n junction straddles the rib waveguide and performs active carrier removal.

to the screening of the applied field by the free carriers. This results in an increase of the effective lifetime and the concomitant reduction in the net gain. Fig. 7 shows the carrier lifetime variation as a function of the optical intensity in the waveguide. The results are obtained through numerical simulations of carrier transport using ATLAS, a computer-aided design tool. At low intensities, the reverse bias is effective in reducing the carrier lifetime. However, at high optical intensities, the lifetime increases due to the screening effect. This important phenomenon puts an upper limit on the maximum continuous wave output power that can be generated in the near-IR by a silicon Raman laser.

In addition to this, the noise performance of silicon Raman amplifiers and lasers have not yet been quantified. These calculations would be important to ascertain the real impact of the silicon Raman devices.

IV. EXPERIMENTAL RESULTS AT MID-IR WAVELENGTHS

The TPA effect, which is responsible for the creation of free carriers in silicon is found to reduce significantly when pumped at energies less than half the bandgap (wavelength $\sim 2.2 \mu\text{m}$).

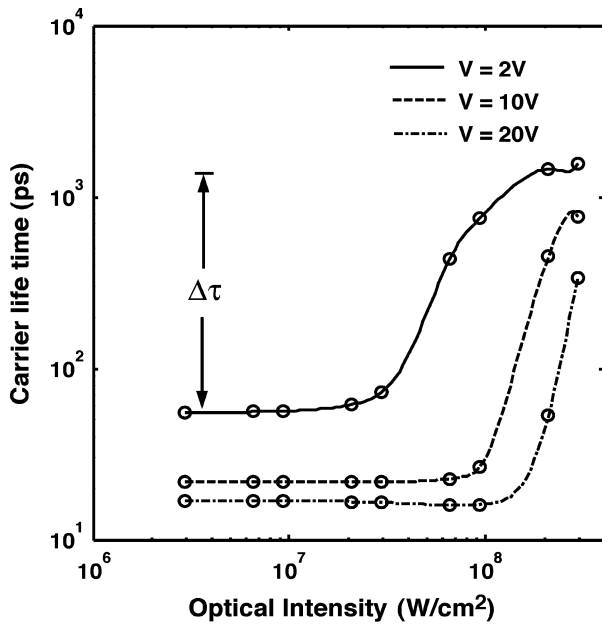


Fig. 7. Variation of lifetime with optical intensity inside the waveguide for different values of reverse voltage. As the intensity is increased, the larger carrier density screens the applied field, and hence prevents carrier sweep out. This leads to an increase in lifetime and, hence, higher optical losses.

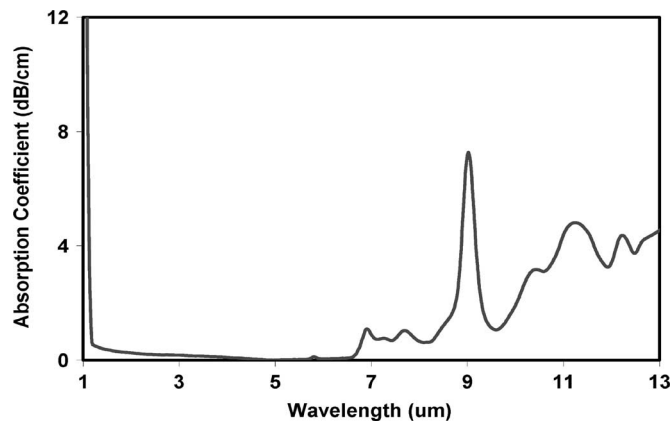


Fig. 8. Linear absorption in silicon measured using an FTIR apparatus.

Two pump photons absorbed simultaneously lack the energy to exceed the energy gap in order to excite electron-hole pairs. The possible nonlinear loss mechanism is the three-PA process and the free carriers associated with the three-PA. This process is much weaker than TPA and is expected to be insignificant at typical pump intensities used to observe Raman nonlinearities. Thus, by employing optical pump in the mid-IR wavelengths, the nonlinear loss mechanisms can be eliminated. This section discusses the experimental results on loss mechanisms at mid-IR wavelengths to support this point.

A. Linear Absorption in Silicon

The linear absorption in silicon was measured using a standard FTIR apparatus. Fig. 8 shows the absorption coefficient of silicon (in decibels per centimeter) as a function of wavelength in the range of 1–13 μm .

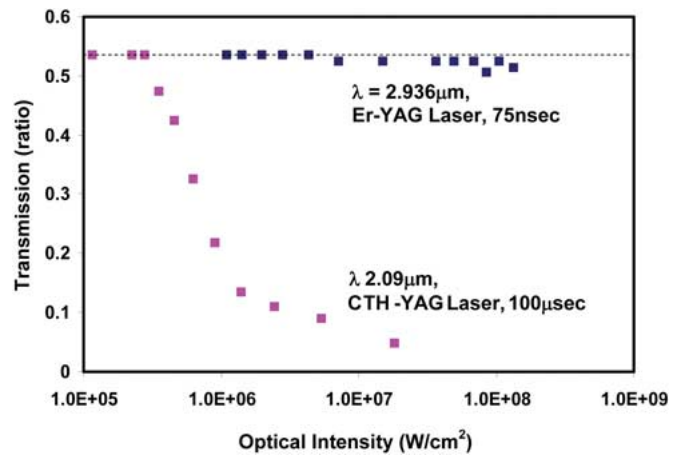


Fig. 9. Optical transmission in silicon as a function of intensity. Two different pump sources at 2.09 and 2.936 μm were used in these experiments. The enhanced nonlinear losses at 2.09 μm due to TPA and FCA, and the absence of these losses at 2.936 μm is clearly seen.

The high losses at around 1 μm can be attributed to the indirect bandgap absorption corresponding to an energy of 1.12 eV. The low-loss window following this absorption peak extends from 1.2 to 6.5- μm wavelength range. This is very attractive for building optical devices in the near IR, telecom, as well as the mid-IR wavelengths. Beyond 7 μm , the increase in losses could be due to multiphonon absorption processes. However, the single-phonon resonance peaks only at 20 μm (or 521 cm^{-1}), and a detailed investigation of these absorption features is necessary.

B. Nonlinear Absorption in Silicon

To measure the nonlinear absorption in silicon as a function of pump intensity, the pulsed pump laser source was coupled into a 1-in thick bulk silicon sample using standard calcium fluoride lens. At the output end, a slow photodetector was used to measure the energy of the pulse. The silicon sample was moved towards the focus of the lens to increase the intensity of the coupled optical beam. The following solid-state pump sources were used in this work: 1) CTH-YAG crystal operating at 2.09- μm , free-running mode with a pulse width of 100 μs and energy of 1 J and 2) Er-doped YAG laser operating at 2.936 μm , Q-switched with a pulse width of 75 ns, and energy of 25 mJ [26].

Fig. 9 shows the transmission through the silicon sample at the pump wavelengths of 2.09 and 2.936 μm . The silicon sample was double-sided polished and the reflection loss per facet is $\sim 29\%$. Hence, the maximum transmission was measured to be $\sim 53\%$.

At 2.09- μm pump wavelength, which is close to the indirect band edge for the TPA process, the transmission reduces considerably with the increasing pump intensity. This loss can be attributed to the TPA and FCA processes. As the energy in pump photons are reduced below half the bandgap, the TPA process is expected to vanish. This is clearly observed in the transmission results corresponding to 2.936- μm pump wavelength. The slight decrease in the transmission with increasing

intensities could be attributed to the three-PA process. However, this process is expected to be extremely weak. Thus pumping beyond the TPA edge (i.e., wavelengths longer than $2.2 \mu\text{m}$) is attractive for building useful nonlinear optical devices with the TPA, and free-carrier loss effects are completely eliminated.

V. DISCUSSION

In this section, the Raman gain achievable using the MWIR pump is estimated, and certain key aspects of the silicon Raman laser design are also discussed. As explained in Section II, the gain-coefficient scales to $1/\lambda_S$ with Stokes wavelength. The gain coefficient of 20 cm/GW at 1550 nm [21] can be extrapolated to the typical MWIR wavelength of $2.936 \mu\text{m}$ achievable using Er-YAG laser [26] to be $\sim 10 \text{ cm/GW}$. The net Raman gain that can be realized at typical pump intensities of 100 MW/cm^2 is $\sim 1 \text{ cm}^{-1}$ or $\sim 4 \text{ dB/cm}$. In the absence of nonlinear loss mechanisms, this gain can be fully utilized to realize laser action in the mid-IR.

One of the motivating factors in studying Raman scattering in silicon waveguides as compared to bulk silicon, is the ability to achieve tight optical confinement, and hence high optical intensities over long interaction lengths. Raman devices operating at mid-IR wavelengths can take advantage of the mature silicon waveguide technology. A suitable low-index cladding is necessary in order to achieve the tight optical confinement. At telecom wavelengths, silicon-on-insulator (SOI) structures with silica as the cladding material has been successfully used in silicon integrated optical devices [27]. However, from the work on optical fibers, it is known that silica becomes highly lossy beyond $1.8 \mu\text{m}$ [23]. Thus, silica is not a suitable cladding for MWIR silicon waveguides. Another requirement of the cladding layer is good thermal conductivity. Sapphire is attractive from the point of view of low index (~ 1.6) and low loss in the MWIR, and good thermal conductivity of $23 \text{ W}\cdot\text{m}^{-1}\cdot\text{K}^{-1}$ (roughly 20 times higher than silica). Fig. 10 is the absorption spectrum of sapphire exhibiting low-loss transmission at the MWIR wavelengths [28]. Thus, silicon-on-sapphire (SOS) structures could be potentially used to build integrated silicon MWIR Raman devices [29].

The stimulated Raman process at high optical intensities is often accompanied by the self-focusing effect, which involves the spatial focusing or defocusing of the optical beam due to the nonlinear refractive index of the medium [11]. In addition to this, the heat dissipated into the Raman medium creates a thermal gradient that alters the refractive index and hence causes lensing effects [11]. These effects have to be included while designing a Raman laser operating at high optical intensities. In a semiconductor Raman medium, the presence of free carriers generated due to TPA also alters the refractive index, and hence causes the lensing effect. This effect is not relevant in silicon at MWIR wavelengths due to the presence of negligible carriers.

The self-focusing effect becomes significant, when it becomes comparable to the diffraction effects of the Gaussian beam in bulk medium [11]. However, when considering Raman scattering in waveguide structures, the optical mode does not diverge because of the guiding achieved by the core-cladding

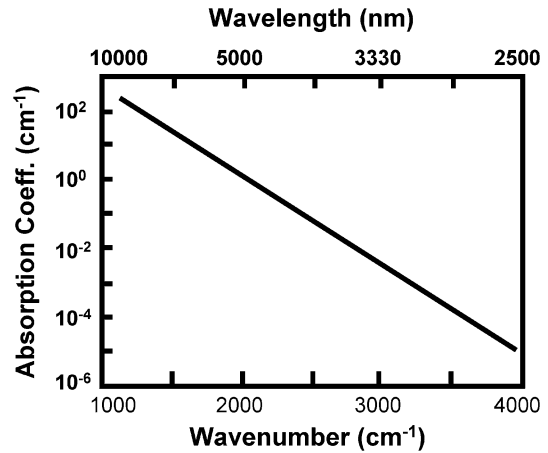


Fig. 10. Absorption spectrum of sapphire versus wavenumber (*lower abscissa*) and wavelength (*upper abscissa*) in the 2500- and 10 000-nm range. Adapted from [28].

index difference. Hence a more relevant parameter that characterizes self-focusing is the index difference induced by the nonlinear refraction in comparison to the core-clad index difference. The index difference causing self-focusing is given as $\Delta n_{sf} = n_2 I$. At typical pump intensities of 100 MW/cm^2 , and $n_2 = 5 \times 10^{-14} \text{ cm}^2/\text{W}$ [30], the change in core index is 5×10^{-6} . Silicon waveguides structures, as discussed later, have much higher core-cladding index difference, hence self-focusing will not have a significant influence on silicon waveguides.

The thermal lensing effect can also be quantitatively evaluated based on the analysis above. Assuming steady-state heat dissipation into the medium, the change in refractive index of the core of the guiding region is given approximately as

$$\Delta n = \frac{dn}{dT} \frac{P_{\text{Heat}} \tau}{\rho C_P V}. \quad (8)$$

The heat dissipated into the medium is the difference in the Stokes and anti-Stokes power [11]

$$P_{\text{Heat}} = P_{\text{Stokes}} \left(\frac{\lambda_S}{\lambda_P} - 1 \right).$$

In silicon, $dn/dT = 1.86 \times 10^{-4}/\text{K}$, density is $\rho = 2.33 \text{ gm/cm}^3$, specific heat is $C_P = 0.7 \text{ J/gm}\cdot\text{K}$, and the thermal relaxation time is $\sim 10\text{--}100 \mu\text{s}$ depending on the cross section over which heat is dissipated. The change in refractive index of the waveguiding region of area $100 \mu\text{m} \times 100 \mu\text{m}$ and length of 1 cm is $\sim 1.14 \times 10^{-4}/\text{W}$ of heat dissipation. This is much smaller than the core-cladding index difference in silicon waveguides, and hence does not cause a significant alteration in the mode profile. Thus, self-focusing and thermal lensing effects that have been found to be important in the design of Raman lasers in bulk materials [11] are not expected to have significant effect in silicon waveguide Raman lasers.

Another interesting feature of the Raman waveguide laser is the possibility of achieving cascaded Stokes emission in nested cavities with the Stokes beam reaching high intensities, and hence acting as a pump for the successive Stokes emission. The

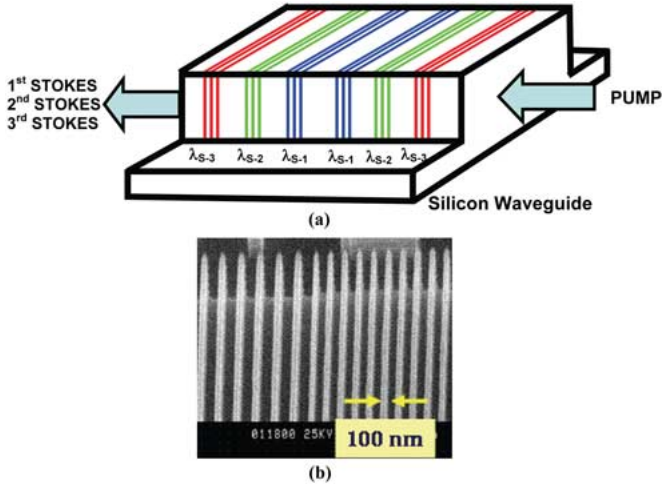


Fig. 11. (a) Integrated cascaded Raman cavity in a silicon waveguide using Bragg mirror pairs to selectively reflect the various orders of the Stokes beam. (b) SEM photograph of chirped Bragg mirrors in silicon fabricated at UCLA using electron beam lithography and deep reactive ion etching.



Fig. 12. Schematic of the integrated cascaded cavity Raman laser using a microresonator structure.

absence of nonlinear loss mechanism will allow higher order Raman emission in a cascaded cavity, extending the addressable wavelength spectrum. Moreover, waveguiding is the key to enable cascaded cavity operation, similar to the cascaded cavity fiber lasers.¹ Figs. 11 and 12 show possible implementation of the integrated cascaded Raman laser cavities. Bragg mirrors can be implemented in silicon by deep etching of one-dimensional (1-D) photonic crystals on the waveguides. The high index of silicon makes it possible to realize high reflection with only a few periods. By implementing such Bragg mirrors for successive Stokes wavelengths, as shown in Fig. 11, it will be possible to achieve cascaded Stokes lasing. The same can also be implemented in a microcavity configuration as shown in Fig. 12. In this case, the successive Stokes wavelengths have to be resonant in the cavity for sustained oscillation. This has been implemented in a silica microcavity in the near IR [31]. Table III lists the successive wavelengths that can be achieved in a cascaded silicon Raman laser. Some tunable laser pump sources

¹Spectra-Physics Telecom: Model RL5 Raman fiber laser specifications.

TABLE III
CASCADED STOKES EMISSION IN A SILICON RAMAN CAVITY. VARIOUS PUMP SOURCES THAT CAN BE USED ARE ALSO LISTED

Pump Wavelength	1st order Stokes	2nd order Stokes	3rd order Stokes
2.1um (CTH:YAG)	2.35um	2.68um	3.12um
2.69um (CTE: YAG)	3.13um	3.74um	4.64um
2.9um (Er:YAG)	3.42um	4.15um	5.30um
2 to 3.5um (CrCdSe)	2.23 to 4.2um	2.52 to 5.37um	2.9 to 7.45um

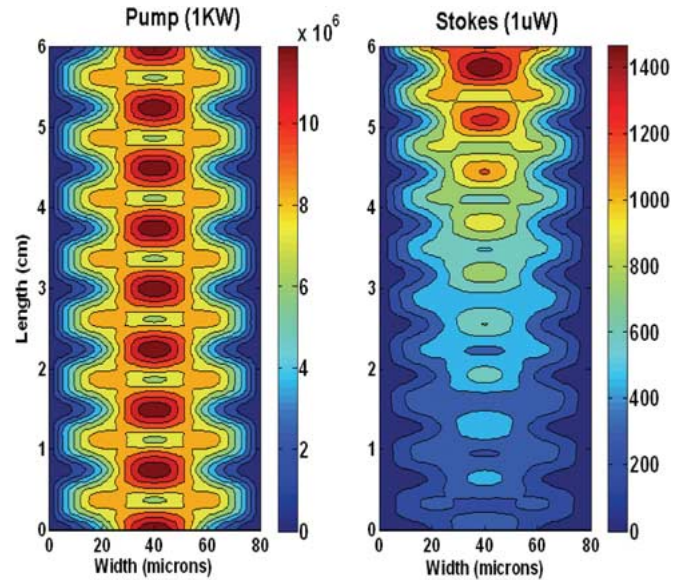


Fig. 13. Contour profile of the electric field amplitude showing the self-imaging Raman amplifier with the evolution of the pump and Stokes along the length of the multimode silicon waveguide [34]. A single pump and Stokes Gaussian beam are launched into the waveguide.

that can operate at wavelengths above the TPA edge of silicon ($\lambda > 2.2 \mu\text{m}$) include the Cr/Tm/Er:YAG laser (cascade emission of ~ 6 laser lines emitted between $2.62\text{--}2.94 \mu\text{m}$), Cr^{+2} and other transition metal-doped ZnSe/ZnS or CdSe laser [continuously tunable from $\sim 2.1\text{--}2.7 \mu\text{m}$ (Cr:ZnSe) or continuously tunable from $\sim 2.1\text{--}3.6 \mu\text{m}$ (Cr:CdSe)] [26], [32], [33].

Raman scattering in multimode waveguides also exhibits some interesting effects. Fig. 13 shows the simulation of a self-imaging Raman amplifier in a multimode silicon waveguide [34]. As shown in this figure, the silicon waveguide amplifies the Stokes signal in the waveguide in the presence of the pump beam, and also periodically reproduces the input image due to Talbot effect. Such an amplifier can find application as an image preamplifier for remote sensing.

VI. CONCLUSION

In summary, silicon Raman lasers should be considered as potential candidates for covering the technologically important MWIR region of the spectrum. The absence of the nonlinear losses, which severely limit the performance of these lasers in the near IR, combined with unsurpassed crystal quality, high-thermal conductivity, and excellent damage threshold render silicon a very attractive Raman medium. Exploiting the mature silicon fabrication technology, low-loss waveguides with long interaction and integrated cascaded microcavities can be employed to realize higher order Stokes emission, and hence to extend the wavelength coverage of the existing pump lasers into MWIR. The proposed technology can expand the application space of silicon photonics beyond data communication, and into biochemical sensing, laser medicine and other MWIR applications.

REFERENCES

- [1] N. P. Barnes, K. E. Murray, M. G. Jani, and S. R. Harrell, "Diode-Pumped Ho, Tm:YLF laser pumping an AgGaSe₂ parametric oscillator," *J. Opt. Soc. Amer. B*, vol. 11, no. 12, pp. 2422–2426, 1994.
- [2] L. E. Myers and W. R. Bosenberg, "Periodically-poled lithium niobate and quasi phase matched optical parametric oscillators," *IEEE J. Quantum Electron.*, vol. 33, no. 10, pp. 1663–1672, Oct. 1997.
- [3] F. Vachss, J. Normans, and C. Turner, "Dual band mid-wave/long-wave IR sources for atmospheric remote sensing," *Proc. SPIE-Int. Soc. Opt. Eng.*, vol. 3533, pp. 174–179, Nov. 1998.
- [4] Y. Ehrlich, S. Pearl, and S. Fastig, "High brightness tunable tandem optical parametric oscillator at 8–12 μm ," presented at the OSA Adv. Solid State Photon. Conf., Santa Fe, NM, Feb. 2004, Paper TuB15.
- [5] M. Vaidyanathan, R. Eckardt, V. Dominic, L. Myers, and T. Grayson, "Cascaded optical parametric oscillations," *Opt. Express*, vol. 1, no. 2, pp. 49–53, 1997.
- [6] S. Chandra, T. H. Allik, G. Catella, R. Utano, and J. A. Hutchinson, "Continuously tunable, 6–14 μm silver-gallium selenide optical parametric oscillator pumped at 1.57 μm ," *Appl. Phys. Lett.*, vol. 71, no. 5, pp. 584–586, 1997.
- [7] D. Rhines, G. Rhines, and P. Moulton, "CdSe OPO pumped by a 2.79 μm Cr:Er:YSGG laser," presented at the OSA Adv. Solid State Photon. (ASSP) Conf., 1995.
- [8] T. H. Allik, S. Chandra, D. M. Rines, P. G. Schunemann, J. A. Hutchinson, and R. Utano, "Tunable 7–12 μm optical parametric oscillator using a Cr:Er:YSGG laser to pump CdSe and ZnGeP₂ crystals," *Opt. Lett.*, vol. 22, no. 9, pp. 597–599, 1997.
- [9] R. K. Shori, N. S. Prasad, and G. Catella, "Demonstration of 4.5–14 μm wavelength generation from Er:YAG laser pumped AgGaSe₂ and CdSe optical parametric oscillators," presented at the Conf. Lasers Electro-Opt. (CLEO), Baltimore, MD, 1999.
- [10] K. L. Vodopyanov, F. Ganikhanov, J. P. Maffetone, I. Zweiback, and W. Ruderman, "ZnGeP₂ optical parametric oscillator with 3.8–12.4 μm tenability," *Opt. Lett.*, vol. 25, no. 11, pp. 841–843, 2000.
- [11] H. M. Pask, "The design and operation of solid-state Raman lasers," *Progr. Quantum Electron.*, vol. 27, pp. 3–56, 2003.
- [12] O. Boyraz and B. Jalali, "Demonstration of a silicon Raman laser," *Opt. Express*, vol. 12, pp. 5269–5273, 2004.
- [13] T. K. Liang and H. K. Tsang, "Role of free carriers from two-photon absorption in Raman amplification in silicon-on-insulator waveguides," *Appl. Phys. Lett.*, vol. 84, no. 15, pp. 2745–2747, 2004.
- [14] R. Claps, V. Raghunathan, D. Dimitropoulos, and B. Jalali, "Influence of nonlinear absorption on Raman amplification in silicon waveguides," *Opt. Express*, vol. 12, pp. 2774–2780, 2004.
- [15] H. Rong, R. Jones, A. Liu, O. Cohen, D. Hak, A. Fang, and M. Pannicia, "A continuous-wave Raman silicon laser," *Nature*, vol. 433, pp. 725–728, 2005.
- [16] B. Jalali, O. Boyraz, D. Dimitropoulos, V. Raghunathan, R. Claps, and P. Koonath, "Silicon Raman amplifiers, lasers, and their applications," in *Proc. 2nd IEEE Int. Conf. Group-IV Photon.*, Sep. 2005, pp. 42–44.
- [17] A. Yariv, *Quantum Electronics*, 3rd ed., New York: Wiley, 1988.
- [18] P. Y. Yu and M. Cardona, *Fundamentals of Semiconductors*, 3rd ed. Berlin, Germany: Springer-Verlag, 2001.
- [19] P. A. Temple and C. E. Hathaway, "Multiphonon Raman spectrum of silicon," *Phys. Rev. A*, vol. 7, pp. 3685–3697, 1973.
- [20] D. Dimitropoulos, B. Housmand, R. Claps, and B. Jalali, "Coupled-mode theory of the Raman effect in silicon-on-insulator waveguides," *Opt. Lett.*, vol. 28, pp. 1954–1956, 2003.
- [21] O. Boyraz, "Silicon Raman lasers, amplifiers and wavelength converters," in *Optical Interconnects: The Silicon Approach*, L. Pavesi and G. Guillot, Eds., Springer Series in Optical Sciences. Berlin, Germany: Springer-Verlag, vol. 119, 2006.
- [22] Y. R. Shen, *The Principles of Nonlinear Optics*. Hoboken, NJ: Wiley, 2003.
- [23] G. P. Agrawal, *Nonlinear Fiber Optics*, 3rd ed. San Diego, CA: Academic, 2001.
- [24] J. R. Sandercock, "Brillouin-scattering measurements on silicon and germanium," *Phys. Rev. Lett.*, vol. 28, pp. 237–240, 1972.
- [25] D. Dimitropoulos, "Nonlinear optics in silicon waveguides at telecom wavelengths" M.S. thesis, Univ. California Los Angeles, Los Angeles, CA, 2003.
- [26] R. K. Shori, A. A. Walston, O. M. Stafsudd, and M. R. Kokta, "Lasing characteristics of free-running and q-switched, high energy 2.69 μm Cr,Tm,Er:YAG laser," *Proc. SPIE*, vol. 3929, pp. 216–221, 2000.
- [27] L. Pavesi and D. J. Lockwood, Eds., *Silicon Photonics*. Berlin, Germany: Springer-Verlag, 2004.
- [28] M. E. Thomas, R. I. Joseph, and W. J. Tropf, "Infrared transmission properties of sapphire, spinel, yttria, and ALON as a function of temperature and frequency," *Appl. Opt.*, vol. 27, no. 2, pp. 239–245, 1988.
- [29] R. A. Soref, S. J. Emelett, and W. R. Buchwald, "Silicon waveguided components for the long-wave infrared region," presented at the Eur. Opt. Soc. Top. Meet. Opt. Microsyst., Capri, Italy, Sep. 2005.
- [30] O. Boyraz, T. Indukuri, and B. Jalali, "Self-phase modulation induced spectral broadening in silicon waveguides," *Opt. Express*, vol. 12, pp. 829–834, 2004.
- [31] T. J. Kippenberg, S. M. Spillane, B. K. Min, and K. J. Vahala, "Theoretical and experimental study of stimulated and cascaded Raman scattering in ultrahigh Q optical microcavities," *J. Sel. Topics Quantum Electron.*, vol. 10, no. 5, pp. 1219–1228, Nov.-Dec. 2004.
- [32] E. Sorokin, S. Naumov, and I. Sorokina, "Ultrabroadband infrared solid state lasers," *J. Sel. Topics Quantum Electron.*, vol. 11, no. 3, pp. 690–712, May/June 2005.
- [33] McKay, K. L. Schepler, and G. C. Catella, "Efficient grating tuned mid-IR Cr²⁺:CdSe laser," *Opt. Lett.*, vol. 24, pp. 1575–1577, 1999.
- [34] V. Raghunathan, R. Rice, and B. Jalali, "A self-imaging silicon waveguide Raman amplifier," submitted to OSA Adv. Solid State Photon. (ASSP) Conf., 2007.



Bahram Jalali (S'86–M'89–SM'97–F'04) received the B.S. degree in physics from Florida State University, Tallahassee, in 1984, and the M.S. and Ph.D. degrees in applied physics from Columbia University, New York, NY, in 1986 and 1989, respectively.

He is currently a Professor of electrical engineering and the Director of the Optoelectronic Circuits and Systems Laboratory at the University of California, Los Angeles (UCLA). From 1988 to 1992, he was a Member of Technical Staff in the Physics Research Division of AT&T Bell Laboratories, Murray Hill, N.J., where he conducted research on ultrafast electronics and optoelectronics. While on leave from UCLA from 1999 to 2001, he founded Cognet Microsystems, a Los Angeles-based fiber-optic component company, where he served as the CEO, President, and Chairman, from inception through its acquisition by Intel Corporation in April 2001. From 2001 to 2004, he served as a Consultant with Intel Corporation. He is on the Board of Trustees of the California Science Center. His current research interests include silicon photonics and ultrafast photonic signal processing. He is the author of over 200 scientific papers and holds six U.S. patents.

Dr. Jalali was chosen by *Scientific American Magazine* as one of the "50 Leaders Shaping the Future of Technology" in 2005. He was the recipient of the BridgeGate 20 Award for his contribution to the southern Californian economy. He is a member of the California Nano Systems Institute (CNSI). He is a Fellow of the Optical Society of America (OSA) and the Chair of the Los Angeles Chapter of the IEEE Lasers and Electro-Optics Society (LEOS).



Varun Raghunathan (S'05) received the B.E. degree in electrical and electronics engineering from Birla Institute of Technology and Science, Pilani, India, in 2002, and the M.S. degree in electrical engineering from the University of California, Los Angeles, in 2005, where he is currently working toward the Ph.D. degree.

His current research interests include experimental study of stimulated Raman amplification, parametric Raman conversion processes, fabrication of silicon photonic structures, nonlinear optics, solid-state physics and quantum electronics.

Mr. Raghunathan was the recipient of the California Nanosystems Institute (CNSI) Graduate Fellowship for Master's studies.



Dimitrios Dimitropoulos received the B.S. degree in electrical engineering from the National Technical University of Athens, Athens, Greece, in 2000. He received the M.S. degree in electrical engineering from the University of California, Los Angeles, in 2003, where he is currently working toward the Ph.D. degree.

His current research focuses on silicon integrated optical devices, particularly silicon Raman lasers, amplifiers, and wavelength converters. His current research interests include areas of quantum electronics

and photonics, noise in physical systems and information theory, and solid-state and plasma physics.



Ramesh K. Shori received the B.S. degree in biology from the University of California, Los Angeles (UCLA), in 1990, the M.S.E.E. degree from Portland State University, Portland, OR, in 1993, and the Ph.D. degree in biomedical engineering from Northwestern University, Evanston, IL, in 2000.

He is currently a Staff Researcher Engineer and a Lecturer in the Department of Electrical Engineering at UCLA. His current research interests include growth and characterization of laser materials, development of high-energy short-pulsed eye-safe 3- μm

erbium-based lasers, and 2–12- μm compact tunable sources as well as investigating dynamic laser-tissue interactions in the UV and IR spectrum for both therapeutic and diagnostic applications.



Oscar Stafsuud (SM'80) received the B.S., M.S., and Ph.D. degrees in physics from the University of California, Los Angeles (UCLA), in 1959, 1961, and 1967, respectively in all physics.

Since 1967, he has been a Faculty member in the Department of Electrical Engineering at ULCA. He has consulted for various corporations such as Hughes Research Laboratories, Nortec Industries, Bendix Advanced Research Laboratory, Litton Industries, Airtron Industries, and Phraxos Research Development. His current research interests include

quantum electronics, especially infrared lasers and nonlinear optics, and solid-state infrared detectors. He holds several patents.

Prof. Stafsuud is a member of the Optical Society of America and the American Association of Crystal Growth.



Sasan Fathpour (S'01–M'04) received the B.S. and M.A.Sc. degrees in electrical engineering from Isfahan University of Technology, Isfahan, Iran, and the University of British Columbia, Vancouver, BC, Canada, in 1995 and 2000, respectively. He received the Ph.D. degree in electrical engineering from the University of Michigan, Ann Arbor, in 2005.

From 1995 to 1997, he was with Isfahan Optics Industry and was engaged in research and development of microelectronic circuits and digital signal processing systems with Pardisan Inc. in 1998. He

is currently a Postdoctoral Research Fellow in the Optoelectronic Circuits and Systems Laboratory at the University of California, Los Angeles. His current interests include active silicon photonic devices based on nonlinear optical effects, such as Raman effect and Kerr effect. His latest accomplishment is the first demonstration of two-photon photovoltaic effect in silicon. His earlier research was focused on epitaxial growth, fabrication, characterization and modeling of In(Ga)As self-assembled quantum dot lasers, with record high dynamic and static performances, spin-polarized light sources based on diluted magnetic III–V semiconductors, and nitride heterojunction bipolar transistors. He is the coauthor of more than 40 papers published in various journals and conference proceedings.